A&A 462, 101–106 (2007)
DOI: 10.1051/0004-6361:20066430

Astronomy & Astrophysics

The proper motion of the Local Group galaxy IC 10

A. Brunthaler[1], M. J. Reid[2], H. Falcke[3,4], C. Henkel[1], and K. M. Menten[1]

[1] Max-Planck-Institut für Radioastronomie, Auf dem Hügel 69, 53121 Bonn, Germany
e-mail: brunthal@mpifr-bonn.mpg.de
[2] Harvard-Smithsonian Center for Astrophysics, 60 Garden Street, Cambridge, MA 02138, USA
[3] ASTRON, Postbus 2, 7990 AA Dwingeloo, The Netherlands
[4] Department of Astrophysics, Radboud Universiteit Nijmegen, Postbus 9010, 6500 GL Nijmegen, The Netherlands

Received 22 September 2006 / Accepted 25 October 2006

ABSTRACT

We have measured the proper motion of the Local Group galaxy IC 10 with the Very Long Baseline Array by measuring the position of an H_2O maser relative to two background quasars over 4.3 years. After correction for the rotation of the Milky Way and IC 10, we obtain a motion of -39 ± 9 μas yr^{-1} toward the East and 31 ± 8 μas yr^{-1} toward the North. This corresponds to a total space velocity of 215 ± 42 km s^{-1} relative to the Milky Way for an assumed distance of 660 ± 66 kpc. Assuming that IC 10 and M 33, for which also a proper motion measurement exists, are bound to M 31, we calculate a lower limit for the mass of M 31 of 7.5×10^{11} $M_\odot$.

Key words. astrometry – galaxies: Local Group – galaxies: individual: IC 10 – galaxies: kinematics and dynamics

1. Introduction

Proper motion measurements of Local Group galaxies are important for our understanding of the dynamics and evolution of the Local Group. Presently, measurements of extragalactic proper motions by optical telescopes are limited to the most nearby companions of the Milky Way, i.e. the LMC (Jones et al. 1994; Kallivayalil et al. 2006a; Pedreros et al. 2006), the SMC (Kallivayalil et al. 2006b), the Sculptor dwarf spheroidal galaxy (dShp) (Schweitzer et al. 1995; Piatek et al. 2006), the Canis Major dwarf galaxy (Dinescu et al. 2005b), the Ursa Minor dSph (Piatek et al. 2005), the Sagittarius dSph (Dinescu et al. 2005a), the Fornax dSph (Piatek et al. 2002; Dinescu et al. 2004), and the Carina dSph (Piatek et al. 2003). These galaxies are all closer than 150 kpc and show motions between 0.2 and a few milliarcseconds (mas) per year. More distant galaxies, such as galaxies in the Andromeda subgroup at distances of ~800 kpc, have smaller angular motions, which are currently not measurable with optical telescopes.

On the other hand, Brunthaler et al. (2005b) measured the proper motions of two groups of water masers on opposite sides of M 33 at radio frequencies with the NRAO[1] Very Long Baseline Array (VLBA). A comparison of the relative proper motion between the two groups of masers and their expected motions from the known rotation curve and inclination of M 33 led to a determination of a "rotational parallax" (730 ± 168 kiloparsec) for this galaxy. This distance is consistent with recent Cepheid and tip of the red giant branch estimates (Lee et al. 2002; McConnachie et al. 2005) and earlier distance estimates using the internal motions of water masers in the IC 133 region (Greenhill et al. 1993; Argon et al. 2004).

Since the proper motion measurements were made relative to a distant extragalactic background source, the proper motion of M 33 itself could also be determined. This measured proper motion of M 33 is a first important step toward a kinematical model of the Local Group and was used to constrain the proper motion and dark matter content of the Andromeda Galaxy M 31 (Loeb et al. 2005).

Water masers in Local Group galaxies have also been found toward the Magellanic Clouds (e.g. Scalise & Braz 1981) and IC 10 (e.g. Henkel et al. 1986). Other Local Group galaxies were searched, but no additional water masers have been detected (see Brunthaler et al. 2006, and references therein). In this paper we report on VLBA observations of the maser in IC 10 to measure its motion.

The extragalactic nature of IC 10 was first recognized by Mayall (1935). Hubble (1936) proposed that it was likely a member of the Local Group and described it as "one of the most curious objects in the sky". However, observations of IC 10 have been always difficult because of the low Galactic latitude of 3°. IC 10 has been classified as an Ir IV galaxy (e.g. van den Bergh 1999), but Richer et al. (2001) argue that it has more properties of a blue compact dwarf galaxy. It is also the nearest galaxy hosting a small starburst, evidenced by its large number of Wolf-Rayet stars (Massey et al. 1992) and the discovery of 144 H II regions (Hodge et al. 1990). Observations of H I with the Westerbork Synthesis Radio Telescope by Shostak et al. (1989) revealed that IC 10 has a regularly rotating disk surrounded by a counter-rotating outer distribution of gas.

The distance to IC 10 is subject to controversy because of difficulties caused by its low Galactic latitude. Early estimates claim a distance of 1–1.5 Mpc (Roberts 1962) and 3 Mpc (Bottinelli et al. 1972; Sandage et al. 1974). Huchtmeier (1979) argued for a closer distance of 1 Mpc. The most recent determination from multi-wavelength observations of Cepheid variables obtained a distance of 660 ± 66 kpc to IC 10 (Sakai et al. 1999), which we adopt throughout this paper.

IC 10 hosts two known H_2O masers, IC 10-SE and IC 10-NW (Becker et al. 1993). The strong SE-component was

[1] The National Radio Astronomy Observatory is operated by Associated Universities, Inc., under a cooperative agreement with the National Science Foundation.

Table 1. Details of the observations: observing date, observation length t_{obs}, beam size θ and position angle PA.

Epoch	Date	$t_{obs}[h]$	θ [mas]	PA[°]
I	2001/02/09	10	0.53×0.33	–15
I	2001/03/28	10	0.55×0.36	–18
I	2001/04/12	10	0.63×0.37	–5
II	2002/01/12	10	0.59×0.35	–19
II	2002/01/17	10	0.64×0.32	–22
III	2002/10/01	10	0.68×0.38	–12
III	2002/10/11	10	0.61×0.34	–5
IV	2003/12/12	12	0.52×0.33	–15
IV	2004/01/10	12	0.50×0.33	–23
V	2004/08/23	12	0.60×0.51	–2
V	2004/09/18	12	0.54×0.35	–17
VI	2005/06/01	12	0.60×0.50	–11
VI	2005/06/07	12	0.56×0.39	–6

first detected by Henkel et al. (1986) and the whole spectrum of IC 10 showed strong variability since its discovery with flux densities between less than 1 Jy (Becker et al. 1993) and a flare with a (single dish) flux density of 125 Jy (Baan et al. 1994). Even intraday variability has been reported by Argon et al. (1994), but the strong component at $v_{LSR} \approx -324$ km s^{-1} has been persistent until now.

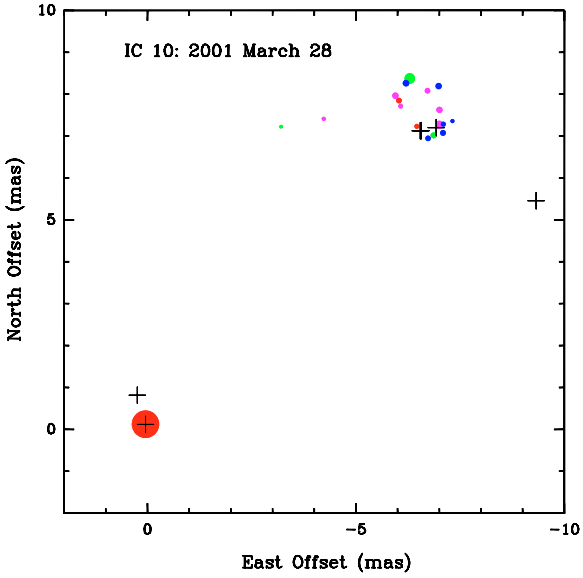

Fig. 1. Composite map of the H_2O masers in IC 10 from 2001 March 28. The area of each circle is proportional to the flux density of the respective component. The colors denote different LSR radial velocities with >-327 km s^{-1} (red), -327 to -330 km s^{-1} (magenta), -330 to -338 km s^{-1} (green), and <-338 km s^{-1} (blue). The crosses mark the positions of the maser emission detected by Argon et al. (1994). The positions were aligned on the strongest maser component in the south-east.

2. Observations and data reduction

We observed the usually brightest maser in IC 10-SE with the VLBA thirteen times between February 2001 and June 2005. The observations are grouped into six epochs, each comprising two closely spaced observations, except the first epoch with three observations, to enable assessment of overall accuracy and systematic errors (Table 1).

We observed in four 8 MHz bands in dual circular polarization. The 128 spectral channels in each band yielded a channel spacing of 62.5 kHz, equivalent to 0.84 km s^{-1}, and covered a velocity range of 107 km s^{-1}. The observations involved rapid switching between the phase-calibrator VCS1 J0027+5958 from the VLBA Calibrator Survey (Beasley et al. 2002), which is a compact background source with continuum emission, and the target sources IC 10 and NVSS J002108+591132. NVSS J002108+591132 is a radio continuum source from the NRAO VLA Sky Survey (NVSS) (Condon et al. 1998) and is located only 8 arcmin from the maser in IC 10. It was also detected in X-rays (Wang et al. 2005) and is most likely also a background quasar. The redshifts of VCS1 J0027+5958 and NVSS J002108+591132 are not known. We switched sources every 30 s in the sequence VCS1 J0027+5958 – IC 10 – VCS1 J0027+5958 – NVSS J002108+591132 – VCS1 J0027+5958 and achieved on-source integration times of ~22 s. The background sources were assumed to be stationary on the sky. Since the phase-calibrator is separated by only 1° on the sky from the target sources, one can obtain precise angular separation measurements.

From the second epoch on, we included *geodetic-like* observations where we observed for 45 min 10–15 strong radio sources (>200 mJy) with accurate positions (<1 mas) at different elevations to estimate an atmospheric zenith delay error in the VLBA calibrator model (see Reid et al. 2004; and Brunthaler et al. 2005a, for a discussion). In the second and third epoch we used two blocks of these geodetic observations before and after the phase-referencing observations. From the fourth epoch on, we included a third geodetic block in the middle of the observation.

The data were edited and calibrated using standard techniques in the Astronomical Image Processing System (AIPS). A-priori amplitude calibration was applied using system temperature measurements and standard gain curves. Zenith delay corrections were performed based on the results of the geodetic-like observations. Data from the St. Croix station were flagged due to high phase noise in all observations. The maser in IC 10 and NVSS J002108+591132 were imaged in AIPS. All detected maser features and NVSS J002108+591132 were unresolved and fit by single elliptical Gaussian components.

3. Results

3.1. Spatial structure

In the first epoch, maser emission could be detected in 21 channels spread over ≈23 km s^{-1}. The spatial distribution of the masers on 2001 March 28 can be seen in Fig. 1. It is similar to the distribution in earlier VLBI observations of IC 10 by Argon et al. (1994). The strongest component at a LSR velocity of ≈−324 km s^{-1} is separated by ≈10 mas or (projected) 6600 AU from the weaker components. This suggests that the emission is associated with a single object if the maser emission is similar to H_2O maser emission in Galactic star forming regions like W3(OH), W49 or Sgr B2 (e.g. Reid et al. 1995; Walker et al. 1977; and Kobayashi et al. 1989, respectively). The weaker maser components form an apparent ring-like structure with a projected size of ≈1.6 mas or 1060 AU.

3.2. Variability

The correlated flux density of the strong feature at –324 km s^{-1} LSR velocity increased from 1.0 to 1.5 Jy between the first two

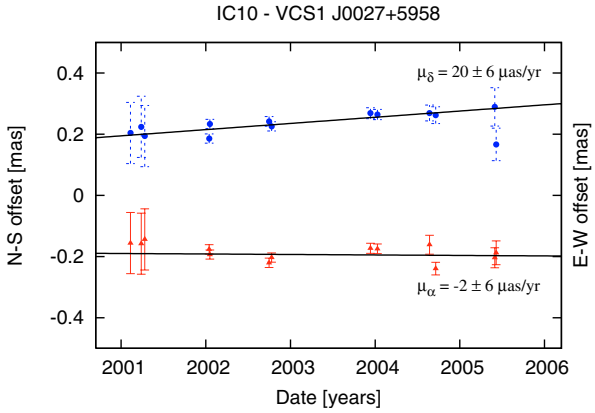

Fig. 2. The position of the maser in IC 10 relative to the phase-reference source VCS1 J0027+5958 in East-West (red triangles) and North-South (blue circles). The lines show a variance weighted linear fit to the data points.

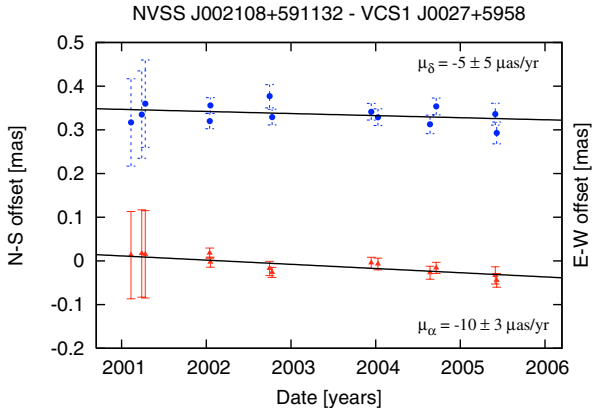

Fig. 3. The position of NVSS J002108+591132 relative to the phase-reference source VCS1 J0027+5958 in East-West (red triangles) and North-South (blue circles). The lines show a variance weighted linear fit to the data points.

VLBA observations of the first epoch. The weaker components are also very variable and they can appear or disappear between observations. In the observations of the second epoch, the flux density of the strongest component was ∼1.1 Jy and some of the weaker components disappeared. In the third epoch, we detected only the strong component with a flux density of ∼0.7 Jy while the weak ring-like structure was not detected anymore. In the later epochs, the flux density of the remaining component dropped to ∼0.2 Jy, 0.12 Jy, and 0.07 Jy in the fourth, fifth, and sixth epoch, respectively.

3.3. Observed motions

The position offsets of the strongest maser feature in IC 10 are shown in Fig. 2. The uncertainties in the observations of the first epoch are larger than the others, because no geodetic-like observations were done to compensate the zenith delay errors. A rectilinear motion was fit to the data and yielded a value of -2 ± 6 μas yr^{-1} toward the East and 20 ± 6 μas yr^{-1} toward the North.

The position offsets of NVSS J002108+591132 are shown in Fig. 3. A rectilinear motion was fit to the data and yielded a motion of -10 ± 3 μas yr^{-1} toward the East and -5 ± 5 μas yr^{-1} toward the North. Hence, NVSS J002108+591132 shows a small but potentially significant motion in right ascension. The apparent motion of NVSS J002108+591132 could be caused by unknown systematic errors.

The phase calibrator VCS1 J0027+5958 may have unresolved structure, e.g. a core-jet structure. The observed image of the source is the convolution of the source structure and the synthesized beam of the VLBA. Flux density variations of the individual components could move the position of the observed image by a fraction of the beam size. Since the phase calibrator is assumed to be stationary, this would shift the positions of all target sources by the same amount.

The observed motion of NVSS J002108+591132 could also be caused by some errors in the geometry of the correlator model (i.e. antenna positions, earth orientation parameters). These errors would be similar for closely spaced observations, but different for observations separated by several months. The angular separation between IC 10 and NVSS J002108+591132 (8′) is much smaller than the separation between IC 10 and VCS1 J0027+5958 (1°), and the position shift induced by geometric errors would be similar for IC 10 and NVSS J002108+591132.

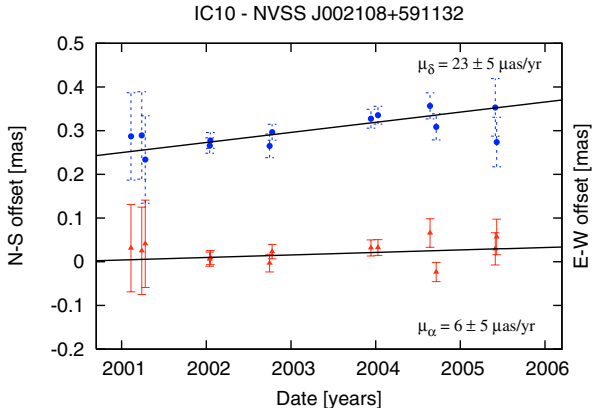

Fig. 4. The position of the strongest maser feature in IC 10 relative to NVSS J002108+591132 in East-West (red triangles) and North-South (blue circles). The lines show a variance weighted linear fit to the data points.

In both cases, the motion of the maser in IC 10 relative to NVSS J002108+591132 would be a better estimate of the proper motion of IC 10. However, it cannot be ruled out that the apparent motion of NVSS J002108+591132 is caused by an unresolved core-jet structure in NVSS J002108+591132 itself. Since strong sources are expected to show more jet-structure than weak sources, amplitude variations of VCS1 J0027+5958 (70–290 mJy) are larger than those in NVSS J002108+591132 (6–11 mJy), and the angular separation between IC 10 and NVSS J002108+591132 is much smaller than the separation between IC 10 and VCS1 J0027+5958, we consider NVSS J002108+591132 as the better astrometric reference source. Figure 4 shows the position of the strongest maser component in IC 10 relative to NVSS J002108+591132. A rectilinear motion was fit to the data and yielded a motion of 6 ± 5 μas yr^{-1} toward the East and 23 ± 5 μas yr^{-1} toward the North and we will adopt these values for the proper motion of the maser.

4. Discussion

4.1. Space motion of IC 10

The measured proper motion $\tilde{\boldsymbol{v}}_{\rm prop}$ of the maser in IC 10 can be decomposed into a sum of several components, relative to a frame at rest at the center of the Milky Way:

$$\tilde{\boldsymbol{v}}_{\rm prop} = \boldsymbol{v}_{\rm rot} + \boldsymbol{v}_{\rm pec} + \boldsymbol{v}_{\odot} + \boldsymbol{v}_{\rm IC\,10}. \quad (1)$$

Here $\boldsymbol{v}_{\rm rot}$ is the motion of the masers due to the internal galactic rotation in IC 10, $\boldsymbol{v}_{\rm pec}$ is the peculiar motion of the masers relative to circular galactic rotation and $\boldsymbol{v}_{\odot}$ is the apparent motion of IC 10 caused by the rotation of the Sun about the Galactic Center. The last contribution $\boldsymbol{v}_{\rm IC\,10}$ is the true proper motion of the galaxy IC 10.

The H_2O masers in IC 10 are located within a massive H I cloud in the central disk. If one assumes that the masers are rotating with the disk, one can calculate its expected proper motion. Shostak et al. (1989) measure an inclination of 45° from the ellipticity of its H I distribution. The masers are 33 arcsec (106 pc) east and 99 arcsec (317 pc) south of the kinematic center. Unfortunately no position angle of the major axis was given. Wilcots et al. (1998) used higher resolution VLA observations of the H I content of IC 10 to fit a tilted ring model to the velocity field of the disk of IC 10. This model has a separate rotation speed, inclination and position angle for each ring. They find a highly inclined disk in the inner 110 arcsec with a position angle of ≈75° and a rotational velocity of ≈30 km s^{-1}. The position of the kinematic center of their tilted ring model was not given. If one combines the kinematic center of Shostak et al. (1989) with the inclination and position angle of Wilcots et al. (1998), one gets an expected transverse motion for the maser ($\boldsymbol{v}_{\rm rot}$) of 26 and 11 km s^{-1} toward the East and North, respectively.

If one calculates the expected motion for different realistic scenarios (i.e. changing the kinematic center by ±20 arcsec, and the inclination and the position angle of the major axis by ±20°), one gets always transverse motions between 20–30 km s^{-1} toward the East and 5–15 km s^{-1} toward the North. The deviation of the motion of the masers from the galactic rotation is unknown. The radial velocity of the CO gas at the position of the maser in IC 10 is about −330 km s^{-1} (Becker 1990), which is close to the radial velocity of the maser. In our Galaxy peculiar motions of star forming regions can be 20 km s^{-1} as seen in W3(OH) (Xu et al. 2006; Hachisuka et al. 2006). Hence, to be conservative, we adopt values of 25 ± 20 and 10 ± 20 km s^{-1} toward the East and North, respectively. This translates to $\dot{\alpha}_{\rm rot} = 8 \pm 6$ and $\dot{\delta}_{\rm rot} = 3 \pm 6$ μas yr^{-1} at a distance of 660 ± 60 kpc.

The rotation of the Sun about the Galactic Center causes an apparent motion of IC 10. The motion of the Sun can be decomposed into a circular motion of the local standard of rest (LSR) and the peculiar motion of the Sun. The peculiar motion of the Sun has been determined from Hipparcos data by Dehnen et al. (1998) to be in km s^{-1} $U_0 = 10.00 \pm 0.36$ (radially inwards), $V_0 = 5.25 \pm 0.62$ (in the direction of Galactic rotation) and $W_0 = 7.17 \pm 0.38$ (vertically upwards). VLBI measurements of the proper motion of SgrA*, the compact radio source at the Galactic Center, yield a motion of 6.379 ± 0.026 mas yr^{-1} along the Galactic plane (Reid et al. 1999, 2004). Combined with a recent geometric distance estimate of the Galactic Center of 7.62 ± 0.32 kpc (Eisenhauer et al. 2005), one gets a circular velocity of 225 ± 10 km s^{-1} for the LSR.

This motion of the Sun causes an apparent proper motion of 38 ± 4 μas yr^{-1} in Galactic longitude and −6 ± 1 μas yr^{-1} in Galactic latitude (for a distance of 660 kpc and Galactic coordinates of IC 10 of $l = 118.96°$, $b = -3.32°$). Converted to equatorial coordinates, one gets $\dot{\alpha}_{\odot} = 37 \pm 4$ μas yr^{-1} and $\dot{\delta}_{\odot} = -11 \pm 1$ μas yr^{-1}.

The true proper motion of IC 10 is then given by

$$\begin{aligned}\dot{\alpha}_{\rm IC\,10} &= \dot{\tilde{\alpha}}_{\rm prop} - \dot{\alpha}_{\rm rot} - \dot{\alpha}_{\odot} \\ &= (6\,(\pm5) - 8\,(\pm6) - 37\,(\pm4))\ \mu\text{as yr}^{-1} \\ &= -39 \pm 9\ \mu\text{as yr}^{-1} = -122 \pm 31\ \text{km s}^{-1}\end{aligned}$$

and

$$\begin{aligned}\dot{\delta}_{\rm IC\,10} &= \dot{\tilde{\delta}}_{\rm prop} - \dot{\delta}_{\rm rot} - \dot{\delta}_{\odot} \quad (2)\\ &= (23\,(\pm5) - 3\,(\pm6) + 11\,(\pm1))\ \mu\text{as yr}^{-1} \\ &= 31 \pm 8\ \mu\text{as yr}^{-1} = 97 \pm 27\ \text{km s}^{-1}.\end{aligned}$$

The measured systematic heliocentric velocity of IC 10 (−344 ± 3 km s^{-1}, de Vaucouleurs et al. 1991) is the sum of the radial motion of IC 10 toward the Sun and the component of the solar motion about the Galactic Center toward IC 10 which is −196 ± 10 km s^{-1}. Hence IC 10 is moving with 148 ± 10 km s^{-1} toward the Sun.

The proper motion and the radial velocity combined give the three-dimensional space velocity of IC 10. The total velocity is 215 ± 42 km s^{-1} relative to the Milky Way. This velocity vector is shown in the schematic view of the Local Group in Fig. 5. Here, we used Cartesian coordinates, where the Sun is located at the origin and the Galactic Center is located at $(x, y, z) = (7.62,\ 0,\ 0)$ (see Appendix A for details).

4.2. Local group dynamics and mass of M 31

If IC 10 or M 33 are bound to M 31, then the velocity of the two galaxies relative to M 31 must be smaller than the escape velocity and one can deduce a lower limit on the mass of M 31:

$$M_{\rm M\,31} > \frac{v_{\rm rel}^2 R}{2G}. \quad (3)$$

A relative velocity of 147 km s^{-1} – for a zero tangential motion of M 31 – and a distance of 262 kpc between IC 10 and M 31, gives a lower limit of 6.6×10^{11} $M_{\odot}$. One can repeat this calculation for any tangential motion of M 31. The results are shown in Fig. 6 (top). The lowest value of 0.7×10^{11} $M_{\odot}$ is found for a tangential motion of M 31 of –130 km s^{-1} toward the East and 35 km s^{-1} toward the North.

For a relative motion of 230 km s^{-1} between M 33 and M 31 – again for a zero tangential motion of M 31 – and a distance of 202 kpc, one gets a lower limit of 1.2×10^{12} $M_{\odot}$ (Brunthaler et al. 2005b). Figure 6 (top) shows also the lower limit of the mass of M 31 for different tangential motions of M 31 if M 33 is bound to M 31. The lowest value is 4×10^{11} $M_{\odot}$ for a tangential motion of M 31 of –115 km s^{-1} toward the East and 160 km s^{-1} toward the North.

Loeb et al. (2005) find that proper motions of M 31 in negative right ascension and positive declination would have lead to close interactions between M 31 and M 33 in the past. These proper motions of M 31 can be ruled out, since the stellar disk of M 33 does not show any signs of strong interactions. Loeb et al. (2005) used a total mass of M 31 of 3.4×10^{12} $M_{\odot}$ in their simulations. Although simulations with lower masses of M 31 yield weaker interactions, motions in negative right ascension and positive declination are still ruled out.

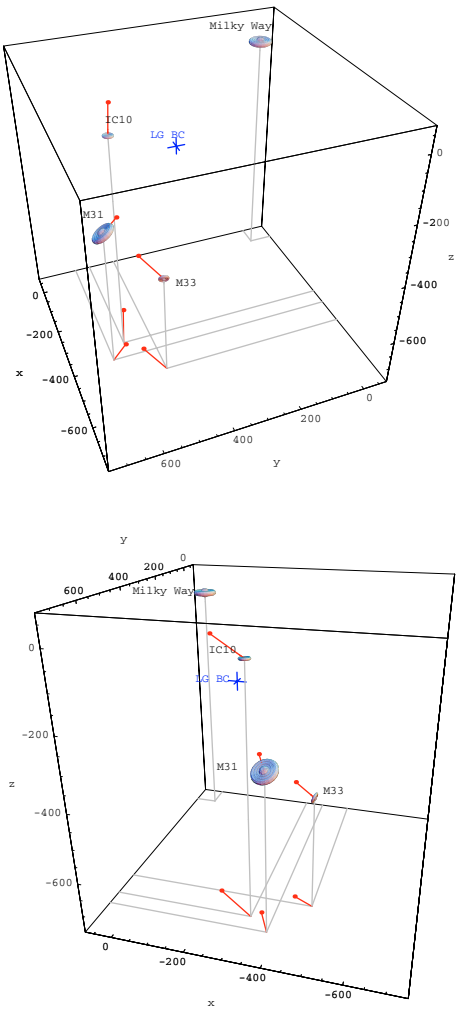

Fig. 5. Schematic view of the Local Group from two viewing angles with the space velocity of IC 10 and M 33 (the latter taken from Brunthaler et al. 2005b) and the radial velocity of Andromeda relative to the Milky Way. The blue cross marks the position of the Local Group Barycenter (LG BC) according to van den Bergh (1999).

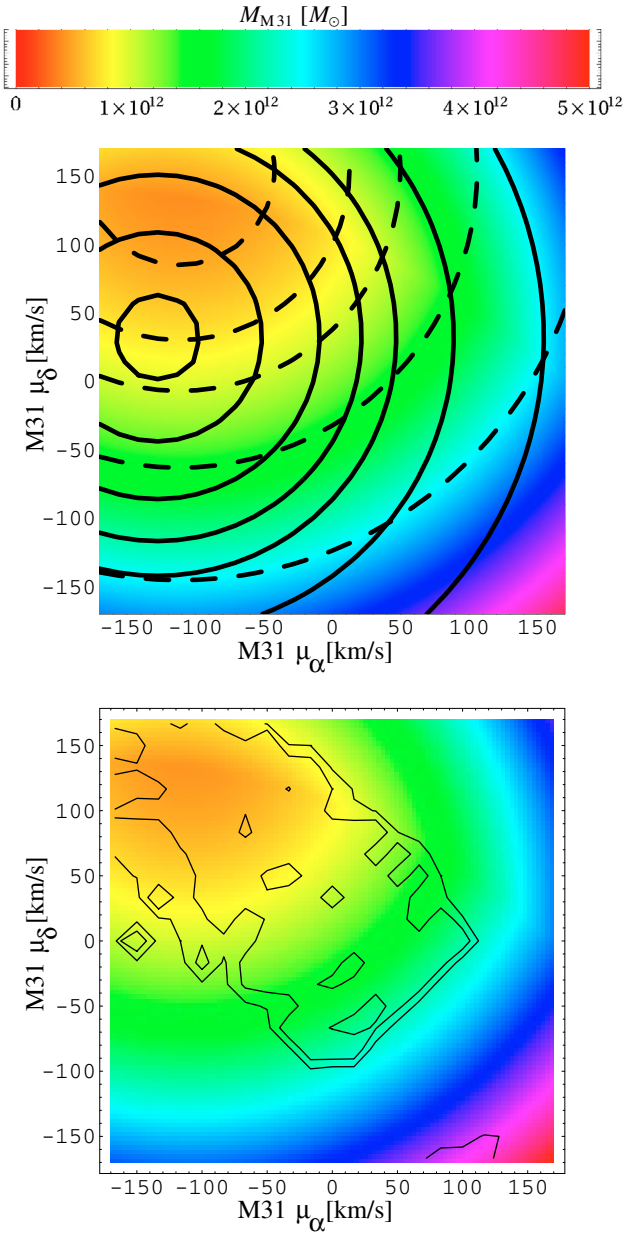

Fig. 6. *Top*: lower limit on the mass of M 31 for different tangential motions of M 31 assuming that M 33 (dashed) or IC 10 (solid) are bound to M 31. The lower limits are (4, 5, 7.5, 10, 15, 25) × 10^{11} $M_\odot$ for M 33, and (0.7, 1, 2.5, 5, 7.5, 10, 15, 25) × 10^{11} $M_\odot$ for IC 10, rising from inside. The colour scale indicates the maximum of both values. *Bottom*: the colour scale is the same as above and gives the lower limit on the mass of M 31. The contours show ranges of proper motions that would have lead to a large ammount of stars stripped from the disk of M 33 through interactions with M 31 or the Milky Way in the past. The contours delineate 20% and 50% of the total number of stars stripped (Loeb et al. 2005). These regions can be excluded, since the stellar disk of M 33 shows no signs of such interactions.

Thus, we can rule out these regions in Fig. 6. This results in a lower limit of 7.5 × 10^{11} $M_\odot$ for M 31 and agrees with a recent estimate of 12.3^{+18}_{-6} × 10^{11} $M_\odot$ derived from the three-dimensional positions and radial velocities of its satellite galaxies (Evans et al. 2000).

5. Summary

We have presented astrometric VLBA observations of the H_2O maser in the Local Group galaxy IC 10. We detected a ring-like structure in one epoch with a projected diameter of ∼1060 AU. We measured the proper motion of the maser relative to two background quasars. Correcting for the internal rotation of IC 10 and the rotation of the Milky Way this measurement yields a proper motion of -39 ± 9 μas yr^{-1} toward the East and 31 ± 8 μas yr^{-1} toward the North, which corresponds to a total space velocity of 215 ± 42 km s^{-1} for IC 10 relative to the Milky Way. If IC 10 and M 33 are bound to M 31, one can calculate a lower limit of the mass of M 31 of 7.5 ×10^{11} $M_\odot$.

Acknowledgements. This research was supported by the DFG Priority Programme 1177.

Appendix A: Coordinate transformations

We define a Cartesian coordinate system where the Sun is located at the origin. To convert from Galactic to Cartesian coordinates, we used

$$\begin{pmatrix} x \\ y \\ z \end{pmatrix} = \begin{pmatrix} R\cos l\cos b \\ R\sin l\cos b \\ R\sin b \end{pmatrix}, \quad \text{(A.1)}$$

where R is the distance, l is the Galactic Longitude, and b is the Galactic Latitude.

To convert the proper motions in right ascension ($\dot{\alpha}$) and declination ($\dot{\delta}$) into proper motions in Galactic Longitude ($\dot{l}$) and Galactic Latitude ($\dot{b}$), we used

$$\begin{pmatrix} \dot{l} \\ \dot{b} \end{pmatrix} = \begin{pmatrix} \cos\theta & \sin\theta \\ -\sin\theta & \cos\theta \end{pmatrix} \begin{pmatrix} \dot{\alpha} \\ \dot{\delta} \end{pmatrix}, \tag{A.2}$$

where θ is the required rotation angle at the position of the source (i.e. $\theta_{\rm IC\,10} = -6.94°$, $\theta_{\rm M\,33} = -348.95°$, $\theta_{\rm M\,31} = -2.74°$).

To compute the velocities in Cartesian coordinates, we constructed for each source three orthogonal vectors $\boldsymbol{e}_r$, $\boldsymbol{e}_l$, and $\boldsymbol{e}_b$ given by

$$\boldsymbol{e}_r = \begin{pmatrix} x \\ y \\ z \end{pmatrix}; \quad \boldsymbol{e}_l = \begin{pmatrix} \frac{y}{x} \\ -1 \\ 0 \end{pmatrix}; \quad \boldsymbol{e}_b = \boldsymbol{e}_r \times \boldsymbol{e}_l. \tag{A.3}$$

These vectors can be normalized to give three orthogonal unit vectors $\hat{\boldsymbol{e}_r}$, $\hat{\boldsymbol{e}_l}$, and $\hat{\boldsymbol{e}_b}$. Then the total velocity $\boldsymbol{v}_{\rm tot}$ of an object with proper motions $\dot{l}$, $\dot{b}$, and the radial velocity $v_{\rm rad}$ is

$$\boldsymbol{v}_{\rm tot} = \dot{l}\,\hat{\boldsymbol{e}_l} + \dot{b}\,\hat{\boldsymbol{e}_b} + v_{\rm rad}\hat{\boldsymbol{e}_r}. \tag{A.4}$$

References

Argon, A. L., Greenhill, L. J., Moran, J. M., et al. 1994, ApJ, 422, 586
Argon, A. L., Greenhill, L. J., Moran, J. M., et al. 2004, ApJ, 615, 702
Baan, W. A., & Haschick, A. 1994, ApJ, 424, L33
Beasley, A. J., Gordon, D., Peck, A. B., et al. 2002, ApJS, 141, 13
Becker, R. 1990, Ph.D. Thesis
Becker, R., Henkel, C., Wilson, T. L., & Wouterloot, J. G. A. 1993, A&A, 268, 483
Bottinelli, L., Gouguenheim, L., & Heidmann, J. 1972, A&A, 18, 121
Brunthaler, A., Reid, M. J., & Falcke, H. 2005a, Atmosphere-Corrected Phase-Referencing, in Future Directions in High Resolution Astronomy, ASP Conf. Ser., 340, 455
Brunthaler, A., Reid, M. J., Falcke, H., Greenhill, L. J., & Henkel, C. 2005b, Science, 307, 1440
Brunthaler, A., Henkel C., de Blok, W. J. G., et al. 2006, A&A, 457, 109
Condon, J. J., Cotton, W. D., Greisen, E. W., et al. 1998, AJ, 115, 1693
de Vaucouleurs, G., de Vaucouleurs, A., Corwin, H. G., et al. 1991, Third Reference Catalogue of Bright Galaxies (Berlin Heidelberg New York: Springer-Verlag), 1, 2069
Dehnen, W., & Binney, J. J. 1998, MNRAS, 298, 387
Dinescu, D. I., Keeney, B. A., Majewski, S. R., & Girard, T. M. 2004, AJ, 128, 687
Dinescu, D. I., Girard, T. M., van Altena, W. F., & López, C. E. 2005a, ApJ, 618, L25
Dinescu, D. I., Martínez-Delgado, D., Girard, T. M., et al. 2005b, ApJ, 631, L49
Eisenhauer, F., Genzel, R., Alexander, T., et al. 2005, ApJ, 628, 246
Evans, N. W., & Wilkinson, M. I. 2000, MNRAS, 316, 929
Greenhill L. J., Moran, J. M., Reid, M. J., Menten, K. M., & Hirabayashi H. 1993, ApJ, 406, 482
Hachisuka, K., Brunthaler, A., Menten, M. K., et al. 2006, ApJ, 645, 337
Henkel, C., Wouterloot, J. G. A., & Bally, J. 1986, A&A, 155, 193
Hodge, P., & Lee, M. G. 1990, PASP, 102, 26
Hubble, E. P. 1936 (Yale University Press)
Huchtmeier, W. K. 1979, A&A, 75, 170
Jones, B. F., Klemola, A. R., & Lin, D. N. C. 1994, AJ, 107, 1333
Kallivayalil, N., van der Marel, R. P., Alcock, C., et al. 2006a, ApJ, 638, 772
Kallivayalil, N., van der Marel, R. P., & Alcock, C. 2006b, ApJ, 652, 1213
Kobayashi, H., Ishiguro, M., Chikada, Y., et al. 1989, PASJ, 41, 141
Lee, M. G., Kim, M., Sarajedini, A., Geisler, D., & Gieren, W. 2002, ApJ, 565, 959
Loeb, A., Reid, M. J., Brunthaler, A., & Falcke, H. 2005, ApJ, 633, 894
Massey, P., Armandroff, T. E., & Conti, P. S. 1992, AJ, 103, 1159
Mayall, N. U. 1935, PASP, 47, 317
McConnachie, A. W., Irwin, M. J., Ferguson, A. M. N., et al. 2005, MNRAS, 356, 979
Pedreros, M. H., Costa, E., & Méndez, R. A. 2006, AJ, 131, 1461
Piatek, S., Pryor, C., Olszewski, E. W., et al. 2002, AJ, 124, 3198
Piatek, S., Pryor, C., Olszewski, E. W., et al. 2003, AJ, 126, 2346
Piatek, S., Pryor, C., Bristow, P., et al. 2005, AJ, 130, 95
Piatek, S., Pryor, C., Bristow P., et al. 2006, AJ, 131, 1445
Reid, M. J., Argon, A. L., Masson, C. R., Menten, K. M., & Moran, J. M. 1995, ApJ, 443, 238
Reid, M. J., & Brunthaler, A. 2004, ApJ, 616, 872
Reid, M. J., Readhead, A. C. S., Vermeulen, R. C., & Treuhaft, R. N. 1999, ApJ, 524, 816
Richer, M. G., Bullejos, A., Borissova, J., et al. 2001, A&A, 370, 34
Roberts, M. S. 1962, AJ, 67, 431
Sakai, S., Madore, B. F., & Freedman, W. L. 1999, ApJ, 511, 671
Sandage A., & Tammann, G. A. 1974, ApJ, 194, 559
Scalise, E., & Braz, M. A. 1981, Nature, 290, 36
Schweitzer, A. E., Cudworth, K. M., Majewski, S. R., & Suntzeff, N. B. 1995, AJ, 110, 2747
Shostak, G. S., & Skillman, E. D. 1989, A&A, 214, 33
van den Bergh, S. 1999, A&AR, 9, 273
Walker, R. C., Burke, B. F., Johnston, K. J., & Spencer, J. H. 1977, ApJ, 211, L135
Wang, Q. D., Whitaker, K. E., & Williams, R. 2005, MNRAS, 362, 1065
Wilcots, E. M., & Miller, B. W. 1998, AJ, 116, 2363
Xu, Y., Reid, M. J., Zheng, X. W., & Menten, K. M. 2006, Science, 311, 54